Systematic Fuel Cavity Asymmetries in Directly Driven Inertial Confinement Fusion Implosions

R. C. Shah, B. M. Haines, F. J. Wysocki, J. F. Benage, J. A. Fooks, V. Glebov, P. Hakel, M. Hoppe, I. V. Igumenshchev, G. Kagan, R. C. Mancini, F. J. Marshall, D. T. Michel, T. J. Murphy, M. E. Schoff, K. Silverstein, C. Stoeckl, and B. Yaakobi

Phys. Rev. Lett. **118**, 135001 — Published 30 March 2017

DOI: 10.1103/PhysRevLett.118.135001

Systematic Fuel Cavity Asymmetries in Directly Driven ICF Implosions

R. C. Shah,[1,*] B. M. Haines,[1] F. J. Wysocki,[1] J. F. Benage,[2] J. Fooks,[3] V. Glebov,[4] P. Hakel,[1] M. Hoppe,[3] I. V. Igumenshchev,[4] G. Kagan,[1] R. C. Mancini,[5] F. J. Marshall,[4] D. T. Michel,[4] T. J. Murphy,[1] M. E. Schoff,[3] K. Silverstein,[4] C. Stoeckl,[4] and B. Yaakobi[4]

[1]*Los Alamos National Laboratory, Los Alamos, NM 87545*
[2]*Sandia National Laboratories, Albuquerque, NM 87123*
[3]*General Atomics, San Diego, CA 92121*
[4]*Laboratory for Laser Energetics, University of Rochester, Rochester, NY 14623*
[5]*Department of Physics, University of Nevada, Reno, Nevada 89557*

(Dated: February 21, 2017)

We present narrow-band self-emission x-ray images from a titanium tracer layer placed at the fuel-shell interface in 60-laser-beam implosion experiments at the OMEGA facility. The images are acquired during deceleration with inferred convergences of ∼9-14. Novel here is that a systematically observed asymmetry of the emission is linked, using full sphere 3-D implosion modeling, to performance-limiting low mode asymmetry of the drive.

PACS numbers: 52.57.Fg

In the field of inertial confinement fusion (ICF), MJ scale lasers, such as the National Ignition Facility (NIF) [1], are being investigated as a path to create self-sustained fusion burn of hydrogen plasma. A small spherical target containing the hydrogen is imploded, with an important objective being that the drive pressure is amplified so as to satisfy the conditions for self-heating. The direct-drive (DD) approach, in which the laser directly ablates the capsule, is being developed using experiments at the 30 kJ OMEGA facility [2]. An obstacle for the DD path to ignition is that the sub-scale OMEGA experiments saturate at a pressure two-fold below the minimum required for ignition, if scaled for the NIF [3]. Long-wavelength asymmetries have been postulated as the cause, but their role has been inferred on the basis of spatially integrated measurements [4]. In this Letter we present a study of directly laser-driven ICF implosions in which we have used x-ray self-emission of a tracer to visualize, with specificity, the asymmetry of the fuel-cavity. By virtue of the technique asymmetry of shape is discovered which suggests that systematic, i.e. shot-to-shot repeatable, character of the on-target laser drive is limiting the achievable pressure.

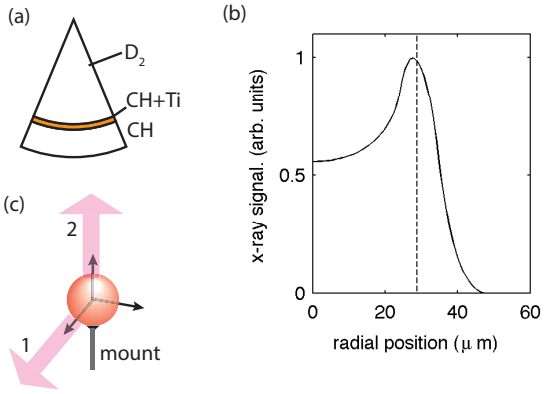

FIG. 1. (a) Self-emission of Ti dopant is used to selectively characterize the shell surface directly in contact with fuel during deceleration. (b) Chord-integrated 5.4-6.0 keV Ti emission from 1-D simulation of capsules with initial 0.1 μm thick, 1% by atom Ti tracer layer. Image is calculated for 40 ps gate beginning 100 ps prior to nuclear bang-time. Dashed vertical line indicates position of fuel-shell interface. (c) Data are presented in the manuscript for views both orthogonal and opposite to mounting.

The importance of implosion symmetry relates to the challenging requirements on pressure with limited laser energy [5]. For self-heating to occur a central "hot-spot" region with temperature ∼5 keV must have areal density of the plasma $\rho R \sim 0.3$ g/cm^2 where ρ is the hot-spot mass density and R its radius. Higher density, and thus increased pressure P reduces the total energy as $E \sim P^{-2}$. The required pressures far exceed the drive ablation pressure (by a factor of $\sim$ 1000) and are obtained from the transfer of kinetic energy of imploding high density fuel/shell into the central low-density hot-spot. As this imploding shell of mass decelerates, temperature, density and consequently pressure of the hot-spot increase. Asymmetries, depending on their mode (often referenced to the spherical harmonic basis), will impact this pressure amplification. Numerical modeling has shown that $\ell \sim 1$ character can rapidly degrade hot-spot pressure due to incomplete stagnation and a de-centering of the pressure profile [4, 6, 7]. In the OMEGA implosion, low modes which impact pressure might result from large target offset [4] or intrinsic aspects of the power balance suggested by x-ray conversion measurements [8]. Numerous published measurements of OMEGA implosions have diagnosed asymmetry of shell areal density and of fuel conditions in nominal implosions through the use of nuclear and x-ray diagnostics [9–12]. Attention has been lacking though with respect to the origin and impact of the low mode asymmetries.

In this Letter we present direct connections between observed low-mode asymmetries and their inferred impact. The measurements rely on a novel imaging technique, which enhances signatures from variations at the perimeter of the fuel-cavity. To do this, a fine Ti-CH tracer layer is selectively placed only at the innermost surface of the ablator (Fig. 1(a)). As the capsule decelerates, core conditions heat the Ti dopant to ∼keV temperatures and it emits into spectral lines originating from He and H-like ions. From the spectrally resolved images of the self-emission we first identify capsule mounting, predicted as a small perturbation on performance. More importantly, a second systematically repeating asymmetry is argued as strong evidence for a drive asymmetry substantially degrading hot-spot pressure. Using full sphere 3-D simulations [4] the impact of drive asymmetry inferred from recently updated x-ray conversion measurements is modeled for our target [8]. The inclusion of the asymmetry accounts for the measured underperformance and, unique to our dataset, provides an explanation for the mode 1 signature in the images.

The targets consist of spherical plastic shells with an outer diameter of 875 μm and 20 μm wall thickness which were diffusion filled so as to hold 10 or 15 atm D_2. The innermost 100 nm of the CH is doped with Ti at 1% by atom (Fig 1(a)). Mandral characterizations showed low modes ($\ell < 10$) typically at least 2× lower than the inner surface specification used in the ignition campaign at NIF [13]. Maximal variations in wall thickness were nominally 0.1-0.2 μm. Targets were mounted randomly, that is to say without any regard to the orientation of their intrinsic asymmetries.

The targets were imploded in the 60 beam geometry at OMEGA [2] with 23 kJ total energy in a 1 ns square laser pulse. For the data presented, all beams were on target with σ_{RMS} ∼3% in energy (typical). Standard approaches were employed to minimize single beam nonuniformities, and facility neutron diagnostics provided the basic performance characterizations of neutron yield, $Y_{\rm n}$, and burn-weighted-ion-temperature, $\langle T_{\rm i}\rangle_{\rm n}$ [14]. Measured Y_n from the $\mathrm{D + D \rightarrow {}^3He + n}$ reaction was 30-40% of calculations assuming 1-D behavior with measured $\langle T_{\rm i}\rangle_{\rm n}$ higher than such ideal calculations by 60%.

The choice of laser pulse will determine shell compressibility defined by the ratio of P/P_F where P_F is the Fermi pressure. Lower values of this quantity, termed adiabat, improve 1-D performance but increase susceptibility to hydrodynamic instability [15]. The high-adiabat square pulse was chosen to minimize extraneous physics.

So as to spectrally select for the tracer emission, the images were acquired using an instrument, termed the Multiple Monochromatic Imager (MMI), which combines a pinhole array and a Bragg reflector [16–18]. An advantage of the MMI is that dispersed images can be selectively summed to generate narrow-band images at specific energies. Here we use the band from 5.4-6.0 keV, which encompasses the modest optical thickness He & Ly β emission and results in a composite image averaged over ∼20 independent images at each position. The pictures are acquired using a 40 ps gate x-ray framing camera with an additional 15 ps spread due to the different positions along the strip of each photon energy. Fig. 1(b) shows the radial variation of the tracer emission from a 1-D simulation [19] based on post-processing using a non-local-thermodynamic-equilibrium (NLTE) database of emissivity and opacity for the Ti doped CH [20, 21]. Because of the very thin layer, the emission has low optical thickness ($\tau \sim 0.3$), and the contrast of the limb in the chord-integrated emission is primarily determined by the spatial and temporal resolution of the measurement. The limb peaks near the radial coordinate of the doped interface (dashed-vertical line).

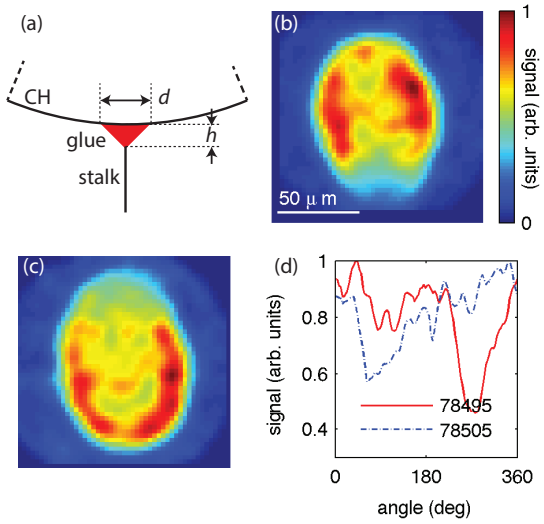

FIG. 2. (a) Omega capsules are positioned at target chamber center using a 17 μm stalk attached to the capsule by a conical glue fillet (typically d=80 μm & h=40 μm) external to the ablator. (b) Gated Ti self-emission extracted from MMI positioned at view #1 (see Fig. 1(c)), with line-of sight orthogonal to mounting and mounting from image-bottom (shot 78495). (c) Image from target inserted from diametrically opposite port such that mounting is from image-top (78505). Images are self normalized. (d) Radially integrated signal variation with angle for images of (b) & (c). Angle increases counter-clockwise around image center with 0° at the 3 o'clock position. Integration at each angle extends from the 20% intensity contour mid-way to the image center, and is length normalized.

As mentioned in the introduction, a systematic asymmetry of OMEGA implosions is expected from mounting, which uses a fiber attached to the target with a conical glue fillet (Fig. 2(a)). In previous simulations (using the 2-D DRACO ICF hydrodynamic code [22]) of low-adiabat implosions the presence of the glue fillet was shown to deform the inbound shock [23]. This then

caused a jetting from the fuel-shell interface with yield degradation specific to the glue parameters. Table I summarizes Y_n from additional DRACO modeling for our implosion over a range of glue parameters and measured yields from experiments (10 atm DD fill). The modeling shows that over this broad parameter range the impact of the asymmetry on yield is modest and varies between ∼10-20%. The experimental yields showed no sensitivity and remained saturated at ∼70% below 1-D, suggesting other causes dominate the current performance.

The jetting nonetheless results in signatures in our imaged Ti emission. A simple correlation study was made with respect to the mounting position, with the images acquired such that the axis of the mount was perpendicular to the line-of-sight (view #1, Fig. 1(c)). Fig. 2(b) shows an MMI image acquired with the mounting from the view bottom whereas for Fig. 2(c) the mounting was inserted from the port 180° opposite, i.e. image-top. The limb brightening anticipated from the 1-D simulation is recognizable but modulated, with a prominent feature being reduction of signal from the mount direction. Fig. 1(d) shows the azimuthal signal variation of the images. Despite competing asymmetries, the signal minimum is nonetheless observed to correlate with the mount orientations of 270° and 90° (0° at 3 o'clock position in the images). This alignment of signal minimum to mount was typical and showed no obvious change with glue parameters. Mounting, while unlikely to explain our yield degradation, is identified as is the predominant cause of mode 1 character from this view [24].

To place the gated MMI images in the context of the implosion trajectory, we have used a comparison between the averaged radii of the 20% intensity contour and the 1-D calculated Ti emission profile. From this analysis, the images of Fig. 2 were determined to be acquired at convergence ratio $C_r \sim 11$ defined by r_i/r_f where $r_{i,f}$ refers to the initial and final radii of the fuel-shell interface. With respect to the simulated 1-D trajectory, this placed the images ∼100 ps prior to peak neutron emission, or bang-time, and roughly halfway through deceleration phase.

In a subsequent campaign we collected data from view #2 of Fig. 1(c). Here, the imager is directly opposite the capsule mounting, and the mounting is thus not expected to perturb the symmetry of the tracer emission. Fig. 3(a-b) show images acquired for two separate shots (15 atm fill, other characteristics as before) with both timed as ∼100 ps prior to bang-time. The repeatability of the prominent mode 1 in Fig. 3(a-b) was typical for this dataset, and the pattern persisted as the implosion reached bang-time, as shown in Fig. 3(c). Averaging three of the later acquisitions, the azimuthal signal variation is ±40% (Fig. 5(a), red-dashed line).

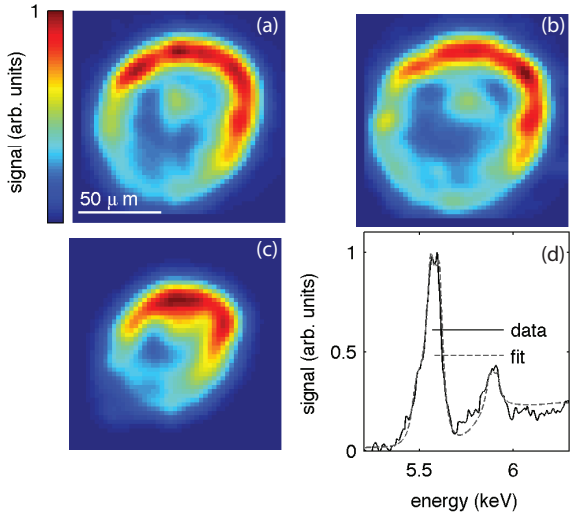

FIG. 3. Data with imager view opposite to capsule mounting, thus minimizing its contribution to observed asymmetry. (a,b) Ti emission images for shot 79972 and 79980 respectively, at ∼100 ps prior to bang-time. (c) Representative image (79980) ∼100 ps later, i.e. at bang-time. (d) Spectrum extracted from MMI gated at bang-time with best-fit from model ($n_e = 5.5 \times 10^{24}$ e/cm^3 and T_e=1350 eV).

Spectral fitting of the tracer line emission is used to ascertain the emissivity averaged electron temperature, T_e, and density, n_e, of the tracer layer. For these near stagnated conditions, the dispersed MMI images were summed to generate a space integrated spectrum [17]. Continuum emission was removed and an exhaustive search was made of n_e, T_e parameter space. The calculated spectra assumed a hollow shell geometry with shell thickness determined from the observed convergence and initial Ti mass. Fig. 3(d) shows the continuum corrected experimental spectrum (solid line) and best fit (dashed line) found from 5.4-6.2 keV for $n_e = 5.5$ $[-1.5, +2.5] \times 10^{24}$ e/cm^3 and $T_e = 1.35$ $[-0.35, +0.15]$ keV. In previous experiments of similar implosions at OMEGA, the spatially averaged conditions in the "mantle" or fuel region adjacent to the fuel-shell interface were found to show near 1-D performance [25]. Given the uncertainties of our data-point, the averaged conditions we have determined might also be considered consistent with

TABLE I. Yield performance from experiment and 2-D simulation for variations of glue fillet dimensions

Mounting Type	d, h (μm)[a]	Simulation $Y_{2\text{-D}}/Y_{1\text{-D}}$ (%)	Experiment[b] $Y_{EXP}/Y_{1\text{-D}}$ (%)
Nominal	80, 40	-	27±2
Increased	110, 55	79	28±2
Reduced	45, 22	93	29±2
None	0, 0	99	-

[a] see Fig. 2(a); these are nominal values for the target types
[b] Determined from 3-4 shots for each type; 10 atm DD fill

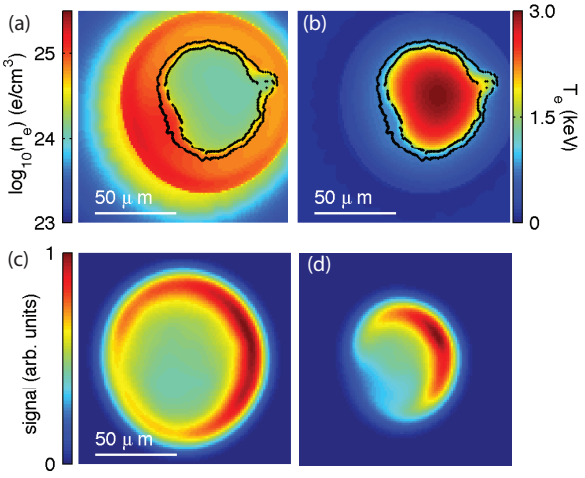

FIG. 4. Results from full sphere 3-D simulation with representative beam-to-beam drive-asymmetry. (a) A cross sectional profile of n_e at nuclear bang-time with Ti-doped CH regions indicated by black contours. An asymmetry of the density profile aligns to the bulk motion of the target. (b) Corresponding profile of T_e. (c) Calculated 5-6 keV self-emission 80 ps prior to and at (d) bang-time.

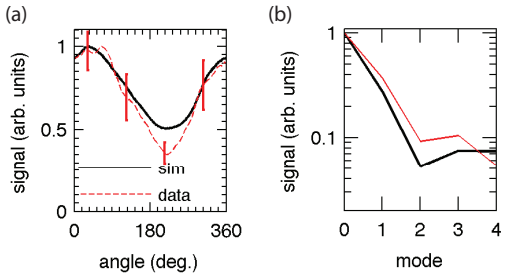

FIG. 5. (a) Comparison of radially integrated emission at bang-time between view #2 measurements (see Fig. 1(c)) and simulation image (Fig 4(d). Signals are phased by aligning their maxima. Error bars on measurement curve indicate standard deviation obtained from three shots. (b) Fourier series analysis of the signals. Mode 1 amplitude is between 20-40 % of signal and at least 4× greater than other modes for both cases.

values extracted from 1-D simulation. However, the images show large variations, or non 1-D dependency, in the emission. From the fitted parameters we conclude we are not observing threshold behavior of the Ti emission. If the tracer layer is assumed at fixed electron pressure (product n_eT_e remains constant), a ±20% change in temperature/density is needed to account for the signal variation [26].

The observed emission modulation from view #2 is linked to drive asymmetry and performance limitations by using the ASTER ICF code [4]. ASTER enables full-sphere 3-D simulations, relevant to asymmetries of Legendre modes $\ell \lesssim 10$. Drive asymmetry is captured by using input power, timing, and pointing of each of the 60 beams. At OMEGA, the power histories of the beams are reported for each shot [14]. However, measurements at high power have inferred that the actual on-target intensity does not follow straightforwardly from these values, with the primary impact being to augment the drive $\ell = 1$ [8]. Recent measurements, which indicate the discrepancy persists, have been used to generate a representative drive map for the ASTER simulation, independent of our imaging measurements. Based on a hard-sphere approximation the measurement-corrected drive contains 2% relative amplitude in $\ell = 1$ (quadrature sum over m modes, calculation using VISRAD 3-D CAD/view-factor software [27]). As such uncontrolled aspects of the OMEGA system will likely drift over extended periods of time, such a drive-map is considered representative only of the magnitude of the low mode asymmetries but not their phasing.

Fig. 4(a,b) show cross-sectional profiles of n_e and T_e at bang-time, in which the black contours indicate the location of the CH-Ti layer. The displacement from center of the profiles indicates a bulk movement due to the $\ell = 1$ in the drive. The tracer layer is at higher density and lower temperature on the over-driven side of the capsule with $\pm \sim 30\%$ low frequency variation in mass averaged conditions. Calculated images with mode 1 character are found over a broad range of observational angles. Examples of synthetic images maximizing mode 1 in emission are shown in Fig. 4(c,d) for acquisitions 80 ps prior to, and at bang-time. The brighter emission is found to correspond to the higher temperature, lower density regions of the tracer. (Synthetic image calculations indicate a negligible role of opacity.) The evolution of the mode 1 in the emission of the synthetic images qualitatively captures the observations shown in the data of Fig. 3(a-c). In Fig. 5(a) the azimuthal variation of the simulated image at bang-time (solid-black) is plotted with the average from experiment (dashed-red). The quantitative levels of mode 1 are comparable (see also modal composition in Fig. 5(b)) thus showing that modeling based on the independent measurements of laser imbalance provides a reasonable explanation for the observations. In the 3-D simulation, the burn weighted pressure falls to ∼50% of 1-D. Y_n is 40% of 1-D, in agreement with the experimental measurement. The much higher experimental $\langle T_i \rangle_n$ of 4.1 keV, as compared to the value of 2.71 keV in the 3-D simulation, is consistent with motional broadening of the measurement resulting from $\ell = 1$ asymmetry [4, 6].

In conclusion, we have used self-emission from a tracer layer to provide strong, novel evidence for low mode drive asymmetry. This drive asymmetry is identified via modeling as a dominant limit on performance.

We acknowledge Omega staff, T. Sedillo, N. Hoffman, K. Prestridge, B.J. Albright, R. A. Gore and S. Batha.

* rcshah@lanl.gov

[1] M. J. Edwards, P. K. Patel, J. D. Lindl, L. J. Atherton, S. H. Glenzer, S. W. Haan, J. D. Kilkenny, O. L. Landen, E. I. Moses, A. Nikroo, R. Petrasso, T. C. Sangster, P. T. Springer, S. Batha, R. Benedetti, L. Bernstein, R. Betti, D. L. Bleuel, T. R. Boehly, D. K. Bradley, J. A. Caggiano, D. A. Callahan, P. M. Celliers, C. J. Cerjan, K. C. Chen, D. S. Clark, G. W. Collins, E. L. Dewald, L. Divol, S. Dixit, T. Doeppner, D. H. Edgell, J. E. Fair, M. Farrell, R. J. Fortner, J. Frenje, M. G. G. Johnson, E. Giraldez, V. Y. Glebov, G. Grim, B. A. Hammel, A. V. Hamza, D. R. Harding, S. P. Hatchett, N. Hein, H. W. Herrmann, D. Hicks, D. E. Hinkel, M. Hoppe, W. W. Hsing, N. Izumi, B. Jacoby, O. S. Jones, D. Kalantar, R. Kauffman, J. L. Kline, J. P. Knauer, J. A. Koch, B. J. Kozioziemski, G. Kyrala, K. N. LaFortune, S. L. Pape, R. J. Leeper, R. Lerche, T. Ma, B. J. MacGowan, A. J. MacKinnon, A. Macphee, E. R. Mapoles, M. M. Marinak, M. Mauldin, P. W. McKenty, M. Meezan, P. A. Michel, J. Milovich, J. D. Moody, M. Moran, D. H. Munro, C. L. Olson, K. Opachich, A. E. Pak, T. Parham, H.-S. Park, J. E. Ralph, S. P. Regan, B. Remington, H. Rinderknecht, H. F. Robey, M. Rosen, S. Ross, J. D. Salmonson, J. Sater, D. H. Schneider, F. H. Sguin, S. M. Sepke, D. A. Shaughnessy, V. A. Smalyuk, B. K. Spears, C. Stoeckl, W. Stoeffl, L. Suter, C. A. Thomas, R. Tommasini, R. P. Town, S. V. Weber, P. J. Wegner, K. Widman, M. Wilke, D. C. Wilson, C. B. Yeamans, and A. Zylstra, Physics of Plasmas **20**, 070501 (2013).

[2] T. Boehly, D. Brown, R. Craxton, R. Keck, J. Knauer, J. Kelly, T. Kessler, S. Kumpan, S. Loucks, S. Letzring, F. Marshall, R. McCrory, S. Morse, W. Seka, J. Soures, and C. Verdon, Optics Communications **133**, 495 (1997).

[3] S. P. Regan, V. N. Goncharov, I. V. Igumenshchev, T. C. Sangster, R. Betti, A. Bose, T. R. Boehly, M. J. Bonino, E. M. Campbell, D. Cao, T. J. B. Collins, R. S. Craxton, A. K. Davis, J. A. Delettrez, D. H. Edgell, R. Epstein, C. J. Forrest, J. A. Frenje, D. H. Froula, M. Gatu Johnson, V. Y. Glebov, D. R. Harding, M. Hohenberger, S. X. Hu, D. Jacobs-Perkins, R. Janezic, M. Karasik, R. L. Keck, J. H. Kelly, T. J. Kessler, J. P. Knauer, T. Z. Kosc, S. J. Loucks, J. A. Marozas, F. J. Marshall, R. L. McCrory, P. W. McKenty, D. D. Meyerhofer, D. T. Michel, J. F. Myatt, S. P. Obenschain, R. D. Petrasso, P. B. Radha, B. Rice, M. J. Rosenberg, A. J. Schmitt, M. J. Schmitt, W. Seka, W. T. Shmayda, M. J. Shoup, A. Shvydky, S. Skupsky, A. A. Solodov, C. Stoeckl, W. Theobald, J. Ulreich, M. D. Wittman, K. M. Woo, B. Yaakobi, and J. D. Zuegel, Phys. Rev. Lett. **117**, 025001 (2016).

[4] I. V. Igumenshchev, V. N. Goncharov, F. J. Marshall, J. P. Knauer, E. M. Campbell, C. J. Forrest, D. H. Froula, V. Y. Glebov, R. L. McCrory, S. P. Regan, T. C. Sangster, S. Skupsky, and C. Stoeckl, Physics of Plasmas **23**, 052702 (2016), http://dx.doi.org/10.1063/1.4948418.

[5] V. N. Goncharov, T. C. Sangster, R. Betti, T. R. Boehly, M. J. Bonino, T. J. B. Collins, R. S. Craxton, J. A. Delettrez, D. H. Edgell, R. Epstein, R. K. Follett, C. J. Forrest, D. H. Froula, V. Yu. Glebov, D. R. Harding, R. J. Henchen, S. X. Hu, I. V. Igumenshchev, R. Janezic, J. H. Kelly, T. J. Kessler, T. Z. Kosc, S. J. Loucks, J. A. Marozas, F. J. Marshall, A. V. Maximov, R. L. McCrory, P. W. McKenty, D. D. Meyerhofer, D. T. Michel, J. F. Myatt, R. Nora, P. B. Radha, S. P. Regan, W. Seka, W. T. Shmayda, R. W. Short, A. Shvydky, S. Skupsky, C. Stoeckl, B. Yaakobi, J. A. Frenje, M. Gatu-Johnson, R. D. Petrasso, and D. T. Casey, Physics of Plasmas **21**, 056315 (2014), http://dx.doi.org/10.1063/1.4876618.

[6] B. K. Spears, M. J. Edwards, S. Hatchett, J. Kilkenny, J. Knauer, A. Kritcher, J. Lindl, D. Munro, P. Patel, H. F. Robey, and R. P. J. Town, Physics of Plasmas **21**, 042702 (2014).

[7] B. M. Haines, F. F. Grinstein, and J. R. Fincke, Phys. Rev. E **89**, 053302 (2014).

[8] F. J. Marshall, J. A. Delettrez, R. Epstein, R. Forties, R. L. Keck, J. H. Kelly, P. W. McKenty, S. P. Regan, and L. J. Waxer, Physics of Plasmas **11** (2004).

[9] V. A. Smalyuk, V. N. Goncharov, J. A. Delettrez, F. J. Marshall, D. D. Meyerhofer, S. P. Regan, and B. Yaakobi, Phys. Rev. Lett. **87**, 155002 (2001).

[10] R. D. Petrasso, J. A. Frenje, C. K. Li, F. H. Séguin, J. R. Rygg, B. E. Schwartz, S. Kurebayashi, P. B. Radha, C. Stoeckl, J. M. Soures, J. Delettrez, V. Y. Glebov, D. D. Meyerhofer, and T. C. Sangster, Phys. Rev. Lett. **90**, 095002 (2003).

[11] H. M. Johns, R. C. Mancini, T. Nagayama, D. C. Mayes, R. Tommasini, V. A. Smalyuk, S. P. Regan, and J. A. Delettrez, Physics of Plasmas **23**, 012709 (2016).

[12] T. Nagayama, *Polychromatic Tomography of High Energy Density Plasmas*, PhD dissertation, University of Nevada, Reno (2011).

[13] S. W. Haan, J. D. Lindl, D. A. Callahan, D. S. Clark, J. D. Salmonson, B. A. Hammel, L. J. Atherton, R. C. Cook, M. J. Edwards, S. Glenzer, A. V. Hamza, S. P. Hatchett, M. C. Herrmann, D. E. Hinkel, D. D. Ho, H. Huang, O. S. Jones, J. Kline, G. Kyrala, O. L. Landen, B. J. MacGowan, M. M. Marinak, D. D. Meyerhofer, J. L. Milovich, K. A. Moreno, E. I. Moses, D. H. Munro, A. Nikroo, R. E. Olson, K. Peterson, S. M. Pollaine, J. E. Ralph, H. F. Robey, B. K. Spears, P. T. Springer, L. J. Suter, C. A. Thomas, R. P. Town, R. Vesey, S. V. Weber, H. L. Wilkens, and D. C. Wilson, Physics of Plasmas **18**, 051001 (2011), http://dx.doi.org/10.1063/1.3592169.

[14] University of Rochester, Laboratory for Laser Energetics, "National Laser Users' Facility Users Guide," `http://www.lle.rochester.edu/media/omega_facility/documentation/documents/nluf_users_guide.pdf` (2007).

[15] P. B. Radha, C. Stoeckl, V. N. Goncharov, J. A. Delettrez, D. H. Edgell, J. A. Frenje, I. V. Igumenshchev, J. P. Knauer, J. A. Marozas, R. L. McCrory, D. D. Meyerhofer, R. D. Petrasso, S. P. Regan, T. C. Sangster, W. Seka, and S. Skupsky, Physics of Plasmas **18**, 012705 (2011), http://dx.doi.org/10.1063/1.3544930.

[16] R. Tommasini, J. Koch, N. Izumi, L. A. Welser, R. C. Mancini, J. Delettrez, S. P. Regan, and V. Smalyuk, in *Proc. SPIE*, Vol. 6317 (2006) p. 631716.

[17] T. Nagayama, R. C. Mancini, R. Florido, R. Tommasini, J. A. Koch, J. A. Delettrez, S. P. Regan, and V. A. Smalyuk, Journal of Applied Physics **109**, 093303 (2011).

[18] B. Yaakobi, F. J. Marshall, and D. K. Bradley, Appl. Opt. **37**, 8074 (1998).

[19] J. MacFarlane, I. Golovkin, and P. Woodruff, Journal of Quantitative Spectroscopy and Radiative Transfer **99**, 381 (2006).

[20] C. J. Fontes, J. Colgan, and J. Abdallah, Jr., in *Modern Methods in Collisional-Radiative Modeling of Plasmas*, edited by Y. Ralchenko (Springer, New York, in press).
[21] C. Fontes, H. Zhang, J. Abdallah, Jr., R. Clark, D. Kilcrease, J. Colgan, R. Cunningham, P. Hakel, N. Magee, and M. Sherrill, J. Phys. B **48**, 144014 (2015).
[22] D. Keller, T. Collins, J. Delettrez, P. McKenty, P. Radha, B. Whiney, and G. A. Moses, in *Bulletin of the American Physical Society, 52nd Annual Meeting of the APS Division of Plasma Physics*, Vol. 44 (1999).
[23] I. V. Igumenshchev, F. J. Marshall, J. A. Marozas, V. A. Smalyuk, R. Epstein, V. N. Goncharov, T. J. B. Collins, T. C. Sangster, and S. Skupsky, Physics of Plasmas **16**, 082701 (2009).
[24] In our experiments, the emission is predominantly from implosion periphery. Due to non-uniformities of this emission we are not able to diagnose jetted material above the base-line signal in the chord integration.
[25] S. P. Regan *et al.*, Phys. Plasmas **9**, 1357 (2002).
[26] Emissivity averaging along line-of-sight may explain why we do not observe changes in MMI images between the He & Ly β emission lines.
[27] J. MacFarlane, Journal of Quantitative Spectroscopy and Radiative Transfer **81**, 287 (2003).